Journal of Catalysis **191,** 12–29 (2000)
doi:10.1006/jcat.1999.2781, available online at http://www.idealibrary.com on IDEAL®

K/Mo Catalysts Supported over Sol–Gel Silica–Titania Mixed Oxides in the Oxidative Dehydrogenation of Propane

Rick B. Watson and Umit S. Ozkan[1]

Department of Chemical Engineering, The Ohio State University, Columbus, Ohio 43210

Received June 29, 1999; revised December 10, 1999; accepted December 10, 1999

The use of silica–titania mixed-oxide-supported molybdenum catalysts has been studied with regard to their activity for the oxidative dehydrogenation of propane. The effect of alkali doping on the catalyst surface characteristics and, in turn, on the catalytic performance has been examined. The catalysts used in this study have been synthesized by a "one-pot" sol–gel/coprecipitation technique.The main focus of the work has been characterization of the surface molybdena species, physical–chemical properties of the Si : Ti support, surface acidity, reducibility, adsorption/desorption behavior, and surface intermediates present during the reaction. Catalysts were characterized by BET surface area measurements, X-ray diffraction, laser Raman spectroscopy, temperature-programmed reduction, X-ray photoelectron spectroscopy, propane temperature-programmed desorption, and diffuse reflectance infrared Fourier transform spectroscopy. By varying the K/Mo molar ratio a maximum in selectivity and yield of propylene was obtained. The maximum yield of propylene obtained in dilute feed experiments was ~30%. Experiments with more concentrated feed mixtures were also performed to achieve a higher percentage of propylene (6–7%) in the product stream.

Key Words: **propane oxidative dehydrogenation; silica–titania mixed oxides; molybdenum; alkali promotion (potassium); DRIFTS; NH_3 adsorption; TPR; TPD; XPS.**

1. INTRODUCTION

Currently, the chemical industry depends heavily on propylene and other alkene feedstocks. Propylene demand is estimated to grow 4.5% per year between 1991 and 2000 (1). The catalytic oxidative dehydrogenation (ODH) of propane is an attractive alternate route for the production of propylene compared to the conventional cracking and dehydrogenation processes. This is because ODH is thermodynamically favored at lower temperatures and usually does not lead to the formation of coke and smaller hydrocarbons. Recent literature has focused on selective, high surface area catalysts active below 823 K. The most selective catalysts reported in recent literature consist of vanadium–magnesium, vanadia supported on niobium, and nickel molybdates (2, 3). In particular, promising results have been obtained when molybdate-based catalysts are promoted or supported.

For example, Ni–Co–Mo (4) V–Nb–Mo/TiO_2 (5), K–$MnMoO_4$ (6), and K_2MoO_4 (7) have shown promise in ODH and other partial oxidation reactions. The positive effect of alkali dopants (Li, Na, K, Rb, and Cs) has long been known in many reactions and is becoming more and more applicable to different catalysts (8). However, the effect is still not well characterized. Alkali doping can have the effect of increasing selectivity and activity while preventing phase transformations, inhibiting sintering, and creating basic centers on the catalyst surface (9). Abello *et al.* have shown a significant increase in selectivity on Mo/MgO–γ-Al_2O_3 with the addition of potassium (10). On this catalyst, an interesting interdependence was noticed among catalyst activity, redox behavior, and surface acidity. Furthermore, past work from our group (6) has shown that potassium can largely enhance oxygen exchange between bulk $MnMoO_4$ catalysts and gas-phase oxygen as well as adsorption/desorption behavior of the catalyst. These parameters are the most common features used to describe ODH catalysts.

Study of silica–titania mixed oxides has gained much attention because of their high activity for epoxidation reactions of olefins with hydroperoxides (11). It has been reported (11) that TiO_2 in mixed oxides of silica and titania can be present not only as anatase, but also in the form of very small domains in which the normal octahedral coordination of TiO_2 has changed to tetrahedral. This leads to the unique structural and chemical properties of this material. Silica–titania mixed oxide supports, through sol–gel preparations, can provide advantages that the respective single oxides cannot. These benefits include stronger metal–support interactions, hindering reduction of the active metal, and smaller particle size that leads to better dispersion and higher surface area. Silica–titania mixed oxides have been studied extensively (12–17) for

[1] To whom correspondence should be addressed. Fax: (614) 292-3769. E-mail: ozkan.1@osu.edu.

0021-9517/00 $35.00

physical–chemical properties such as acidity, porosity, existence of Ti–O–Si chemical bonds, and TiO_2/SiO_2 phase separations. However, few studies have been done on their use as support material for transition metals. Baiker *et al.* (18) and Vogt *et al.* (19) have used vanadia supported on silica–titania mixed oxides for the reduction of nitric oxide with ammonia. Baiker has shown that the addition of titania causes an interaction that prevents agglomeration of surface vanadia species. Udomsak and Anthony (20) have shown a significant difference in isobutane dehydrogenation activity on chromia/silica–titania catalyst with different preparation methods. Hydrogen and carbon monoxide interactions with titania-promoted palladium on silica was studied by Rieck and Bell (21). Here, it was shown that TiO_x species decorate the palladium, causing a notable difference in the CO adsorption behavior. Feng *et al.* (22) have shown the hydrogen abstracting ability of the weakly acidic palladium catalysts supported on silica–titania mixed oxide was the dominating factor for nonoxidative dehydrogenation of propane. To the best of our knowledge, the use of molybdenum as an active metal over silica–titania mixed oxide support for the ODH of propane has not been previously reported.

In this work, the use of silica–titania mixed-oxide-supported molybdenum catalysts has been studied with regard to their activity for the ODH of propane. The effect of alkali doping on the catalyst surface characteristics and, in turn, on the catalytic performance has been examined. The catalysts used in this study have been synthesized by a "one-pot" sol–gel/coprecipitation technique. The main focus of the work has been characterization of the surface molybdena species, physical–chemical properties of the Si : Ti support, surface acidity, reducibility, adsorption/desorption behavior, and surface intermediates present during the reaction. The chemical–physical properties were investigated using several techniques. Surface area and pore size distribution were measured using the BET N_2 adsorption method. X-ray diffraction (XRD), Raman spectroscopy, and X-ray photoelectron spectroscopy (XPS) were used to determine the nature of the Si : Ti support and supported molybdena phases with and without alkali doping. In an attempt to relate catalytic behavior to surface acidity and reducibility, diffuse reflectance FTIR spectroscopy (DRIFTS) of adsorbed ammonia and temperature-programmed reduction (TPR) experiments were performed on the K/Mo catalysts. Furthermore, to examine the adsorption/desorption behavior of the K/Mo catalysts and the nature of the surface intermediates, temperature-programmed desorption (TPD) of adsorbed propane and *in situ* DRIFTS spectroscopy were used. As part of this study, several sol–gel preparation parameters (i.e., hydrolysis procedure, pH, alkoxide concentrations) have also been examined with respect to their effect on the performance of these catalysts in the propane ODH reaction.

2. METHODS

2.1. Catalyst Preparation

Catalysts were prepared using a modified sol–gel/coprecipitation technique. Ammonium heptamolybdate (AHM) (Mallinkrodt) and KOH (Fisher) were used for molybdenum and potassium precursors, respectively. For silica–titania mixed oxides, tetraethylorthosilicate (TEOS) (Aldrich) and titanium(IV) isopropoxide (TIPO) (Aldrich) were used. The solvent was isopropyl alcohol. In this modified sol–gel method, calculated amounts of the silica and titania alkoxide precursors were placed in solvent to yield, after calcination, SiO_2–TiO_2 mixed oxides with the desired molar Si : Ti ratio. This solution was left stirring while an aqueous solution containing the necessary amount of AHM of molybdenum (10% Mo loading) was then added dropwise with a syringe pump. The aqueous solution added contained the stoichiometric amount of water necessary to hydrolyze all of the alkoxide precursors. The aqueous solution was added at a rate of 0.5 cm^3/min for all catalysts with one exception. For the catalyst prepared with fast addition, the aqueous solution was added at a rate of 2 cm^3/min. For catalysts containing potassium, KOH was added to the aqueous solution to give the desired K/Mo molar ratio. For catalysts denoted as prehydrolyzed, the stoichiometric amount of water necessary to hydrolyze the entire silica precursor was added to the silica precursor only and stirred for 15 min before proceeding. For acidic and basic preparations, the effective pH of the alcohol solution was maintained at pH 3 (acidic) and pH 11 (basic) during preparation using HNO_3 and NH_4OH, respectively. Resulting gels were stirred for an additional 15 min after all of the aqueous solution had been added and dried at room temperature for less than 3 h. They were then placed in an oven at 110°C for overnight drying and solvent removal. After drying, the catalysts were ground to a fine powder and calcined under oxygen at 550°C for 5 h. This method is referred to as a "one-pot" sol–gel/coprecipitation because as the silica and titania precursors are hydrolyzed and precipitate out of solution, potassium molybdate species, which are insoluble in alcohol, also precipitate.

Synthesized catalysts are listed in Table 1. Catalysts numbered 1 through 7 are a series of molybdate catalysts with increasing K/Mo molar ratio at constant (10 wt%) loading of Mo and a Si : Ti molar ratio of 1. Catalysts 8 through 11 were prepared keeping K/Mo constant at 2 and varying the silica and titania content. Since TEOS hydrolyzes much more slowly than TIPO, a series of prehydrolyzed catalysts were also prepared. Catalysts 12 through 15 were synthesized using different hydrolysis methods (prehydrolysis of silica precursor, fast or slow addition of the aqueous solution, acidic or basic conditions). Catalysts 16 and 17 refer to a bare silica–titania support and a potassium-doped silica–titania support, respectively.

TABLE 1

Sol–Gel Catalysts and Supports

No.	Composition	Preparation	Surface area (m^2/g)
1	10% Mo/Si : Ti 1 : 1	Coprecip., sol–gel	229
2	10% (K/Mo = 0.07)/Si : Ti 1 : 1	Coprecip., sol–gel	136
3	10% (K/Mo = 0.14)/Si : Ti 1 : 1	Coprecip., sol–gel	121
4	10% (K/Mo = 0.3)/Si : Ti 1 : 1	Coprecip., sol–gel	166
5	10% (K/Mo = 0.6)/Si : Ti 1 : 1	Coprecip., sol–gel	65
6	10% (K/Mo = 1)/Si : Ti 1 : 1	Coprecip., sol–gel	17
7	10% (K/Mo = 2)/Si : Ti 1 : 1	Coprecip., sol–gel	106
8	10% (K/Mo = 2)/SiO_2	Coprecip., sol–gel	156
9	10% (K/Mo = 2)/TiO_2	Coprecip., sol–gel	43
10	10% (K/Mo = 2)/Si : Ti 2 : 1	Coprecip., sol–gel	75
11	10% (K/Mo = 2)/Si : Ti 1 : 2	Coprecip., sol–gel	17
12	10% (K/Mo = 2)/Si : Ti 1 : 1	Acidic prehydrolyzed sol–gel	271
13	10% (K/Mo = 2)/Si : Ti 1 : 1	Fast prehydrolyzed sol–gel	149
14	10% (K/Mo = 2)/Si : Ti 1 : 1	Prehydrolyzed sol–gel	178
15	10% (K/Mo = 2)/Si : Ti 1 : 1	Basic prehydrolyzed sol–gel	179
16	Si : Ti support only	Sol–gel	320
17	K-doped Si : Ti support	Sol–gel KOH (for K/Mo = 2)	380

2.2. Catalyst Characterization

BET surface area measurement and nitrogen adsorption–desorption isotherms were recorded using a Micrometrics AccuSorb 2100E instrument. X-ray diffraction patterns were obtained with a Scintag PAD-V diffractometer using Cu Kα radiation. Raman spectra were recorded with a Dilor spectrometer using the 514.5-nm line of an Innova 300 Ar laser. Spectra were taken in the range 200–1800 cm^{-1} in 180° back-scattering mode with a Spectrum One CCD detector.

Temperature-programmed reduction (TPR). TPR of catalysts was performed using a laboratory-made gas flow system described in detail elsewhere (23). Catalyst samples (100 mg) were placed in a $\frac{1}{4}$-in.-i.d. U-tube quartz reactor and pretreated under an oxygen flow at 550°C for 30 min followed by cooling to room temperature under nitrogen. The reduction was performed with 10% hydrogen in nitrogen (25 cm^3/min.). The thermal conductivity detector (TCD) was operated in differential mode and the signal transferred to a data acquisition computer. The outlet of the reactor was passed through a column of silica gel to remove moisture formed during the reduction. The temperature program was as follows: 10 min at room temperature, 10°/min ramp rate to 850°C, and holding at 850°C for 10 min.

X-ray photoelectron spectroscopy (XPS). XPS of catalysts was performed with a Physical Electronics/Perkin Elmer (model 550) ESCA/Auger spectrometer operated at 15 kV, 20 mA, and using Mg Kα radiation. Spectra were corrected using the C 1*s* signal, located at 284.6 eV. Relative percentages of K_2MoO_4 and MoO_3 in the samples were calculated using the integrals of the deconvoluted Mo 3*d* spectra. The deconvolution of Mo 3*d* spectra was accomplished using linked doublets of equal FWHM, an intensity ratio of 2/3, and a splitting of 3.15 eV.

Diffuse reflectance infrared Fourier transform spectroscopy (DRIFTS). DRIFTS of catalysts was performed using a Bruker IFS66 instrument equipped with a DTGS detector and a KBr beamsplitter. Catalysts were placed in a sample cup inside a Spectratech diffuse reflectance cell equipped with KBr windows and a thermocouple mount that allowed direct measurement of the surface temperature. Room temperature spectra for each catalyst were averaged over 1000 scans in the mid-IR range (400–4000 cm^{-1}) to a nominal 2 cm^{-1} resolution. Prior to collection of spectrum, catalysts were pretreated under 10% oxygen in helium for 30 min at 400°C surface temperature to remove adsorbed water and carbon dioxide. For NH_3 adsorption experiments, background was taken under helium at room temperature. Following background measurement, NH_3 adsorption (0.5% NH_3/He) was performed for 1 h. Spectra were taken after evacuation for 30 min under helium. For *in situ* spectra, background spectra were taken at room temperature and at 450°C sample surface temperature. Gas-phase spectra were taken at 450°C. *In situ* spectra were taken after 15 min to 1 h of exposure to reaction mixture (%N_2/C_3/O_2, 61%/26%/13%). An additional spectrum was recorded once the reaction chamber was quenched to room temperature under nitrogen flow.

Propane *temperature-programmed desorption (TPD)* of catalysts was performed using the same laboratory-made gas flow system described for TPR experiments. Catalyst samples (100 mg) were placed in a $\frac{1}{4}$-in.-i.d. U-tube

quartz reactor and pretreated under oxygen flow at 550°C for 30 min, followed by cooling to room temperature under helium. Samples were flushed with helium for 1 h followed by 1 h of propane adsorption. After adsorption, desorbed species were monitored by a mass spectrometer (HP5890GC-MS) under helium carrier gas. For these studies, the GC columns were replaced by an empty capillary column. The mass spectrometer was equipped with a quadrupole mass analyzer that allows tracking of up to 20 mass-to-charge ratios (m/z) simultaneously in the selected ion mode. Identification of species with equal m/z ratios was accomplished by following characteristic mass fragments of the species. The temperature program was as follows : 10 min at room temperature, 10°/min ramp rate to 700°C, and holding at 700°C for 20 min.

2.3. Oxidative Dehydrogenation of Propane

Steady-state reaction experiments were carried out in a fixed-bed quartz reactor, operated at ambient pressure. The reactor system, shown in Fig. 1, is such that gaseous feed may be directed through $\frac{1}{8}$-in. stainless steel lines into the reactor and furnace assemblies. A HP 5890 series II gas chromatograph equipped with FID and TCD detectors performed separations and analysis of reaction products online. Separations were performed using three columns : (1) Hayesep D (8-ft. × $\frac{1}{8}$-in.) for hydrocarbons and partially oxygenated hydrocarbons; (2) Porapak Q (6-ft. × $\frac{1}{8}$-in.); and (3) molecular sieve 5 Å (6-ft. × $\frac{1}{8}$-in.) for N_2, O_2, CO, CO_2, and H_2O. Catalyst samples, ranging from 0.1 to 1.5 g, were held in place by a quartz frit. The dead volume of the quartz microreactor was filled with quartz wool and/or ceramic beads to minimize effects from any homogeneous reaction/surface-assisted gas-phase reaction and to provide a short residence time for propylene formed. Reaction temperatures ranged from 723 to 823 K. The quartz reactor, both empty and filled with quartz wool/ceramic beads, showed no activity up to 823 K. The feed consisted of propane/oxygen/nitrogen at flows between 10–200 cm^3/min, usually at a flow rate of 25 cm^3/min. The amount of nitrogen was varied for some runs. However, the propane/oxygen molar ratio was held constant at 2. The concentration of

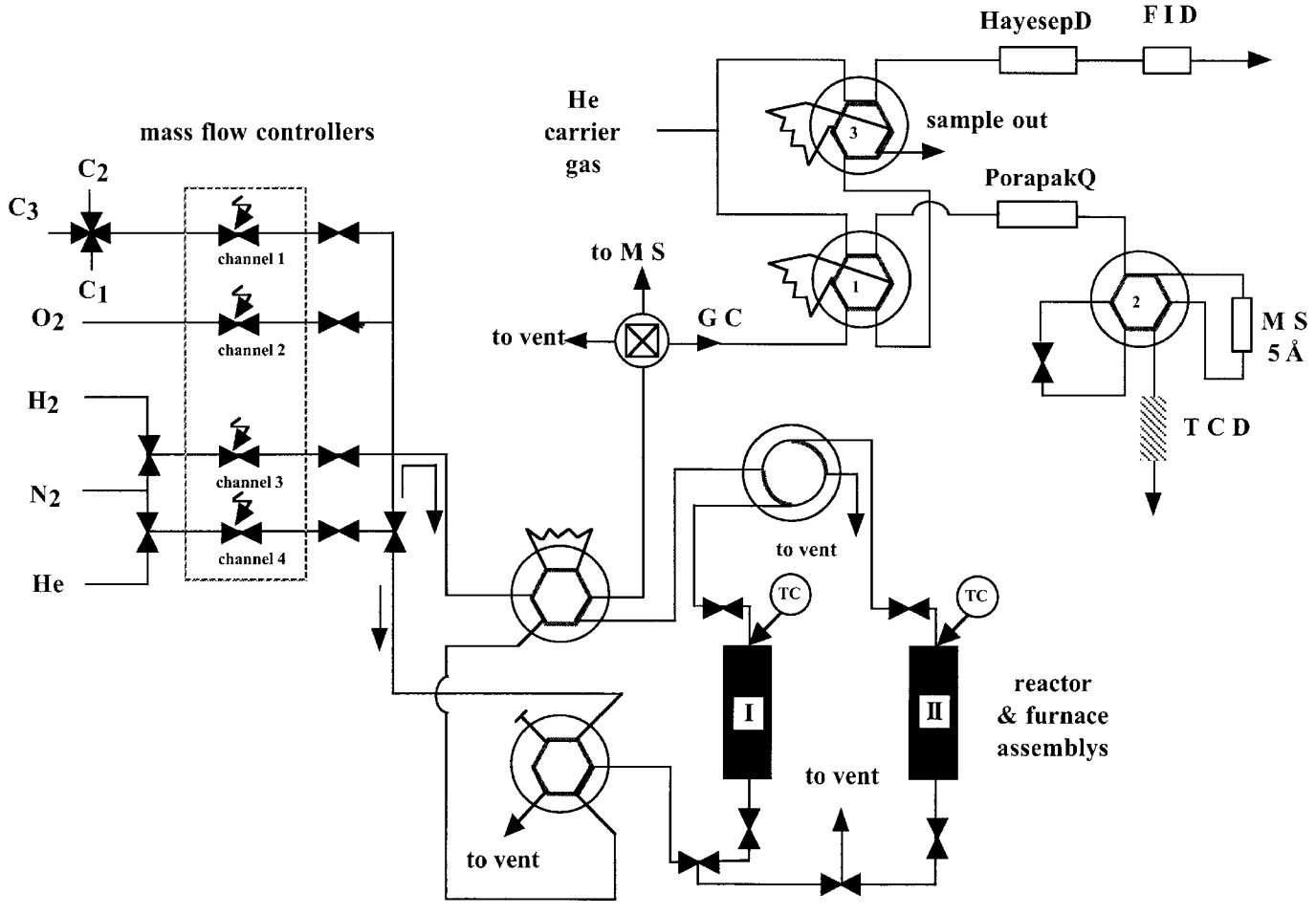

FIG. 1. Schematic of the reactor system.

the feed stream was maintained outside the flammability limits of propane–oxygen–nitrogen mixtures for all runs. The main products of the dehydrogenation reaction were propylene, ethylene, carbon dioxide, carbon monoxide, and water. Acrolein was the only oxygenated product observed, and when present was at the ppm level. The product distributions maintained a carbon balance of 100% (±5%). Conversion is defined as the number of moles of carbon converted divided by the number of moles of carbon present in the feed. Selectivity is defined as the number of moles of carbon in the product divided by the number of moles of carbon reacted.

3. RESULTS

3.1. Catalyst Characterization

Molybdate catalysts show a general decrease in surface area with increasing amounts of potassium added. The catalyst with the K/Mo ratio of 2, however, is somewhat outside this trend. Furthermore, all catalysts containing potassium exhibited lower surface area than the "molybdenum only" catalyst. Comparing catalysts of different Si : Ti contents, it is seen that the highest surface area is achieved with a silica–titania molar ratio 1 : 1. Prehydrolyzed catalysts all show higher surface areas than the catalyst prepared using stoichiometric hydrolysis of both precursors. The effect of potassium on the support is shown to increase the surface area from 320 to 380 m^2/g.

The nitrogen adsorption–desorption isotherm of the Si : Ti 1 : 1 indicated a micro- to mesoporous structure. The pore size distribution was calculated using the desorption isotherm. This yielded an average pore diameter of 2.1 nm and a pore volume of 0.34 cm^3/g.

X-ray diffraction of the Si : Ti 1 : 1 support yielded a pattern typical of a silica–titania sample (25). One broad peak with its center located at a *d* spacing of 3.59 Å was observed, which is the most intense diffraction line from anatase structure. A broad peak is indicative of a finely dispersed, small X-ray particulate anatase structure supported over amorphous silica. With the addition of molybdenum this band becomes narrower. The presence of potassium doping also has an effect on the width of this line, making it narrower with increasing K/Mo ratio. This suggests a change in the dispersion and segregation of titania in the Si : Ti matrix. No molybdenum species can be detected in any of the Si : Ti 1 : 1 catalysts with 10% Mo loading. This indicates that molybdena species are more finely dispersed on these mixed oxide supports than on silica or titania alone. Although quite weak, the two most intense peaks from crystalline molybdenum oxide become noticeable when the Mo loading level is increased to 20%.

Raman spectra of the Si : Ti 1 : 1 support are shown in Fig. 2. The bands associated with anatase structure are shifted to lower wavenumbers than that of pure anatase (11) and appear at 618, 488, and 370 cm^{-1}. The shoulder at 955 cm^{-1} provides some evidence for the Si–O–Ti connectivity as reported in the literature (11). A second band that is associated with the Si–O–Ti bond is at 1100 cm^{-1}. However, this band overlaps with the asymmetric Si–O–Si stretching vibration of 1070 cm^{-1} and is difficult to resolve. Raman spectra of catalysts with different K/Mo ratios are presented in Fig. 3. Present in the spectra are the three bands associated with anatase at ~643, ~523, and ~404 cm^{-1}. These bands are shifted to lower wavenumbers than those of pure anatase and are seen to grow in intensity with increasing K/Mo ratio. An important feature of these spectra is that there is little or no evidence of crystalline MoO_3 since the most intense band characteristic of Mo–O–Mo stretching vibrations in MoO_3 is not present, except as a very weak band on the catalyst with K/Mo = 0.6. The bands associated with isolated terminal Mo=O stretching vibrations are visible in the 970–999-cm^{-1} region. Broad bands arising from surface-coordinated Mo–O–Mo vibrations are located around 850 cm^{-1}. For catalysts K/Mo = 0.6 and 1, there is evidence for higher crystallinity of potassium molybdate species (K_2MoO_4, $K_2Mo_2O_7$) indicated by sharper bands around 900–950 cm^{-1} (26, 27).

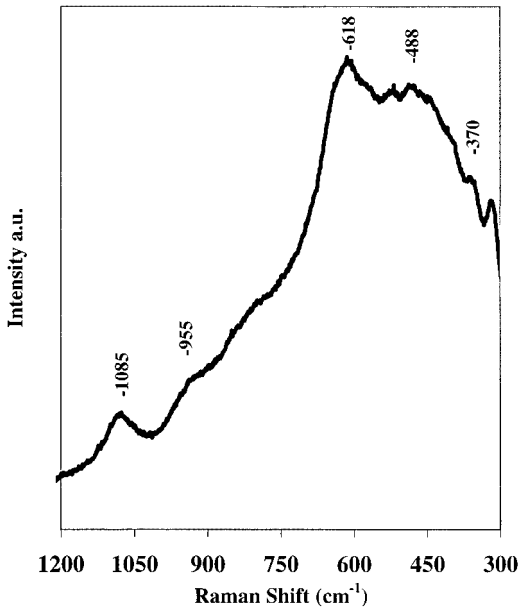

FIG. 2. Raman spectra of Si : Ti 1 : 1 support.

Molybdenum $3d_{5/2}$ binding energies of catalysts with different K/Mo ratios are presented in Table 2. In potassium-containing catalysts, molybdenum exists in two distinct coordination environments. one corresponds to an octahedral MoO_3 matrix and the other to a tetrahedral K_2MoO_4 matrix. Binding energies of bulk MoO_3 and K_2MoO_4 are presented for comparison. When on a Si : Ti 1 : 1 support, our work has shown that Mo 3*d* binding energies shift to a

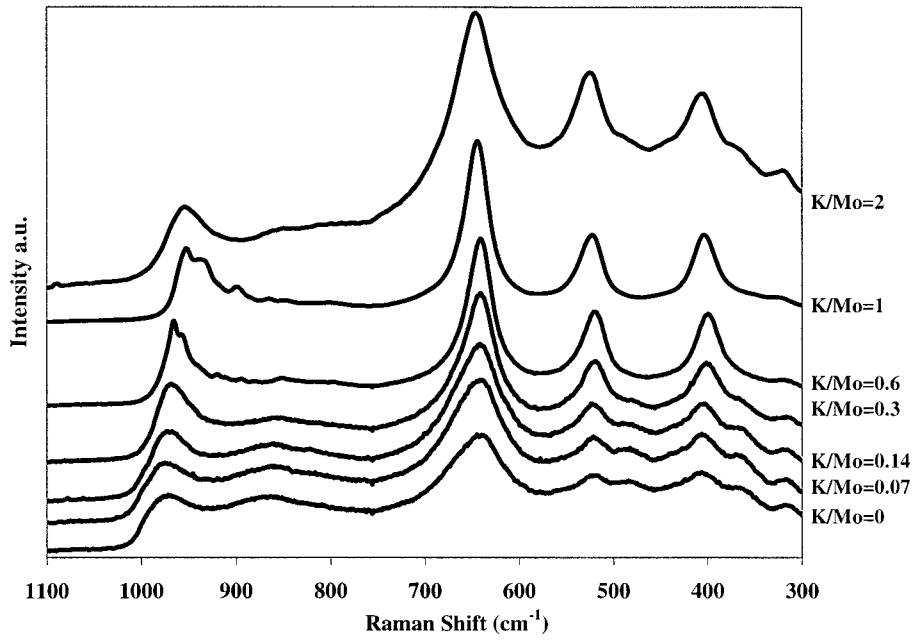

FIG. 3. Raman spectra of 10% Mo/Si : Ti 1 : 1 catalysts with different K/Mo ratios.

lower value when compared to bulk MoO_3. The Mo $3d_{5/2}$ peak for the K/Mo = 0.6 shows the binding energy nearest to that of bulk MoO_3, possibly indicating the presence of three-dimensional MoO_3 regions on this catalyst. The percentages of molybdenum in the MoO_3 matrix, calculated using the deconvoluted peak areas, closely match the "as prepared" compositions. It appears that all of the potassium added to these catalysts exists in a K_2MoO_4 type matrix. Furthermore, K $2p_{3/2}$ spectra show one peak at an average location of 292.5 eV corresponding to that of K_2MoO_4.

To study the change in the nature of the support with K/Mo ratio, Ti $2p_{3/2}$ XPS were taken for catalysts with K/Mo = 0, 0.3, 0.6, and 2. The variation of Ti $2p_{3/2}$ binding energies with increasing K/Mo ratio is presented in Fig. 4. Here, the Ti $2p_{3/2}$ binding energy is seen to shift to lower values with the addition of potassium. The binding energy for the K/Mo = 0 catalyst appears at 459.7 eV indicating that titania is closely interacting with silica and in a state of very small anatase domains (28). The peaks shift to lower binding energies with increasing K/Mo ratios, reaching 458.2 eV for the K/Mo = 2 catalyst. The Ti $2p_{3/2}$ binding energy of pure anatase is around 458.0 eV.

TABLE 2

Mo $3d_{5/2}$ Binding Energies of 10% Mo/Si : Ti 1 : 1 Catalysts with K/Mo Ratios of 0, 0.3, 0.6, and 2

Catalyst	1st Mo $3d_{5/2}$	2nd Mo $3d_{5/2}$
MoO_3	233.4	—
10% Mo/Si : Ti 1 : 1	232.4	231.7
10% (K/Mo = 0.3)/Si : Ti 1 : 1	232.6	231.2
10% (K/Mo = 0.6)/Si : Ti 1 : 1	233.2	232.0
10% (K/Mo = 2)/Si : Ti 1 : 1	232.3	231.6
K_2MoO_4	—	231.8
Catalyst	% MoO_3	% MoO_3 as prepared
10% (K/Mo = 0.3)/Si : Ti 1 : 1	83	85
10% (K/Mo = 0.6)/Si : Ti 1 : 1	74	70
10% (K/Mo = 2)/Si : Ti 1 : 1	5	0

3.2. Reaction Experiments for the Oxidative Dehydrogenation of Propane

Catalysts with K/Mo ratios ranging from 0 to 2 as well as the bare Si : Ti 1 : 1 support were tested in the ODH reaction using equal surface area loading (65 m^2) in the reactor and at temperatures of 450 and 550°C. The feed percentages for these experiments were $N_2/C_3H_8/O_2$ 61%/26%/13%. Variation of propane conversion with K/Mo ratio for these equal surface area tests is presented in Fig. 5. At 450°C, conversion goes through a broad maximum reaching about 21% at K/Mo = 0.07 and falls to zero at K/Mo = 2. At 550°C, variation of conversion shows a similar trend, but this time reaching a maximum of about 33%. The Si : Ti support exhibits a higher conversion than catalysts with K/Mo = 0.6 and above. Table 3 summarizes the product distribution obtained in these experiments. The yield of propylene, which is the major reaction product, mimics the trend observed for conversion, showing a broad maximum with increasing K/Mo ratio. The yield of propylene drops rather drastically at K/Mo ratios higher than 0.6. The support shows fairly high activity compared to high K/Mo ratio catalysts under these feed conditions. The yields of C_2H_4, C_2H_6, and CH_4 are all lower than 1%. At the low K/Mo ratios, the CO yield

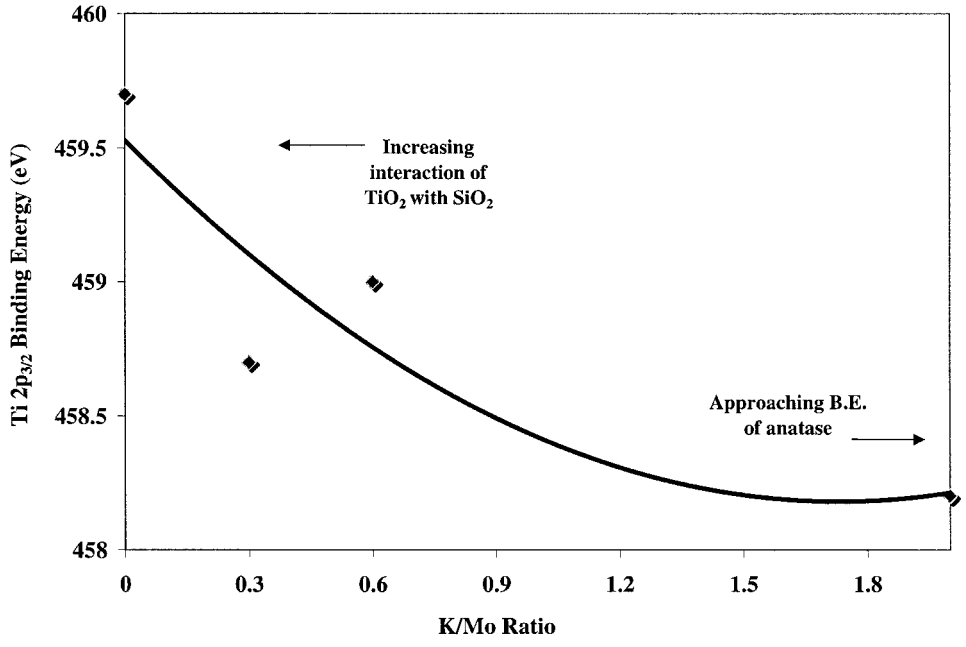

FIG. 4. Variation of titania $2p_{3/2}$ binding energies for 10% Mo/Si : Ti 1 : 1 catalysts with different K/Mo ratios.

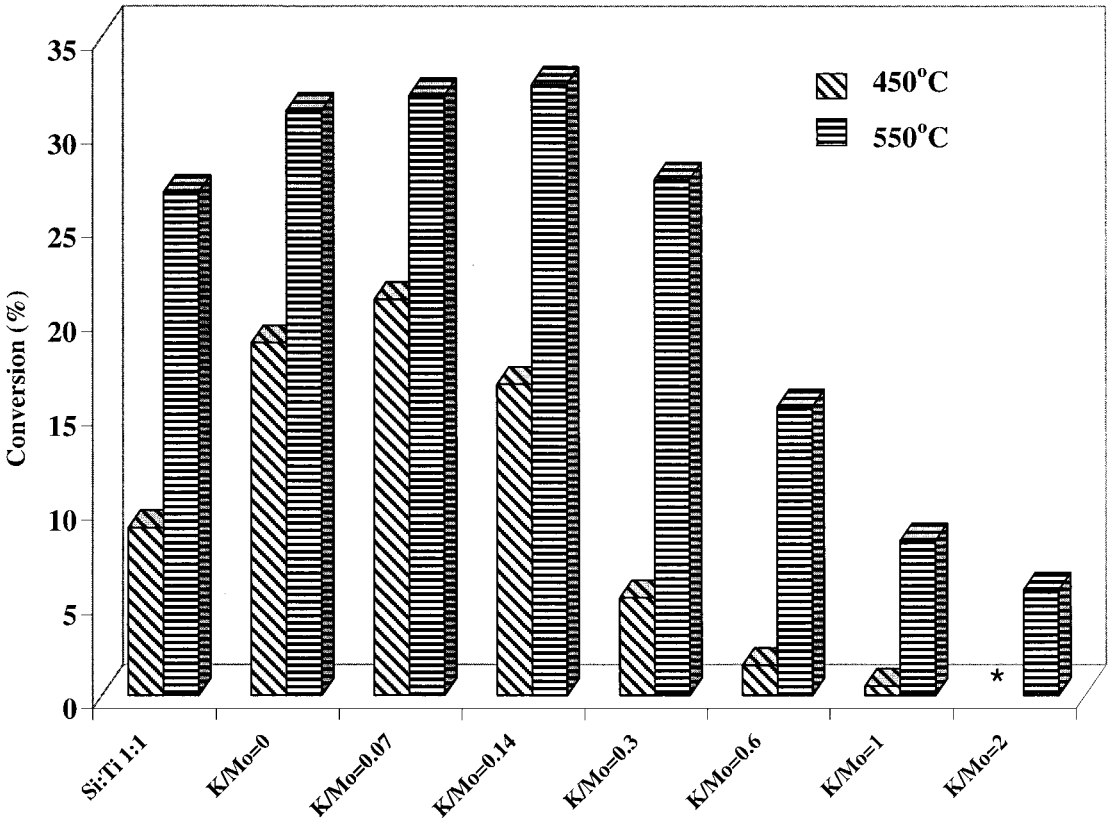

FIG. 5. Conversion of propane for 10% Mo/Si : Ti 1 : 1 catalysts with different K/Mo ratios, equal surface area reactions (65 m^2); $\%N_2/C_3/O_2$, 61%/26%/13%; 25 cm^3/min.

TABLE 3

Reaction Comparison for 10% Mo/Si : Ti 1 : 1 Catalysts with Different K/Mo Ratios

	Yield (%)					
T (°C)	C_3H_6	CO_2	CO	C_2H_4	CH_4	C_2H_6
Si : Ti 1 : 1						
450	6.9	1.2	0.7	0.1	0.0	0.0
550	18.9	3.6	3.6	0.5	0.2	0.0
10% (Mo)/Si : Ti 1 : 1						
450	11.4	2.3	4.9	0.0	0.1	0.0
550	20.0	3.1	6.7	0.4	0.8	0.0
10% (K/Mo = 0.07)/Si : Ti 1 : 1						
450	13.9	2.3	4.8	0.0	0.0	0.0
550	21.2	3.4	6.0	0.4	0.8	0.0
10% (K/Mo = 0.14)/Si : Ti 1 : 1						
450	11.3	1.8	3.4	0.0	0.0	0.0
550	21.4	4.1	5.6	0.0	1.3	0.0
10% (K/Mo = 0.3)/Si : Ti 1 : 1						
450	5.0	0.2	0.0	0.0	0.0	0.0
550	19.9	3.9	2.9	0.4	0.4	0.0
10% (K/Mo = 0.6)/Si : Ti 1 : 1						
450	1.4	0.2	0.0	0.0	0.0	0.0
550	11.5	2.5	0.6	0.6	0.0	0.1
10% (K/Mo = 1)/Si : Ti 1 : 1						
450	0.5	0.0	0.0	0.0	0.0	0.0
550	7.2	0.6	0.0	0.3	0.2	0.0
10% (K/Mo = 2)/Si : Ti 1 : 1						
450			No conversion			
550	4.8	0.6	0.0	0.1	0.1	0.0

Conditions: equal surface area reactions (65 m^2); %$N_2/C_3/O_2$, 61/26/13; 25 cm^3/min.

is higher than the CO_2 yield, but the CO yield drops very rapidly with increasing K/Mo ratio.

To better compare the selectivities of these catalysts, a series of experiments were performed at 450°C, keeping the propane conversion constant at 5% and at 10%. Equal conversion levels were achieved by changing the mass of catalyst loaded. The feed concentrations were the same as those of the equal surface area experiments. Figure 6 shows the variation of propylene selectivities with K/Mo ratio at 5% and 10% conversion levels. The propylene yield goes through a relatively sharp maximum, reaching levels of about 96% and 92% for 5% and 10% conversion, respectively. Table 4 shows the overall product distribution for the equal conversion experiments. It is seen that the carbon monoxide selectivity decreases with the increasing K loading, dropping to zero at K/Mo ratios of 0.6 and above. While CO selectivity drops to zero at these higher K/Mo ratios, we begin to see formation of ethylene and methane.

Parmaliana and co-workers (29) have noted that high yields can be obtained at low propane feed concentrations (<5%), although this may lead to propylene concentrations in the product stream that are rather low for practical separation. However, the need for high-yield catalysts is still the most important consideration for using this process in propylene production. The previously mentioned reaction results were obtained with concentrated feed mixtures ($N_2/C_3H_8/O_2$, 61%/26%/13%) to provide a higher propylene concentration in the product stream. Experiments were also performed using a more dilute propane concentration ($N_2/C_3H_8/O_2$, 92.5%/5%/2.5%). Using this feed concentration, the performances of two of the catalysts with highest propylene selectivity (K/Mo ratios of 0.07 and 0.3) were compared to those of the potassium-free catalyst and of the bare Si : Ti support. Figure 7 shows the yields obtained for different reaction products in this set of experiments. Reaction experiments were run at 550°C using a flow rate of 20 cm^3/min and keeping the catalyst bed volume constant. Under these conditions, the catalyst with a K/Mo ratio of 0.07 gave a propylene yield of ~30%. This experiment was repeated, reproducing the same result with a variation less than ±1%. The yields for catalysts with K/Mo ratio of 0.3 and 0 were 24 and 19%, respectively. The propylene yield over the bare support for this set of experiments was below 2%. The potassium-containing catalysts showed lower yields of CO, CO_2, C_2H_4, CH_4, and C_2H_6 compared to potassium-free catalyst.

Figure 8a shows the effect of residence time on propylene yield over the K/Mo = 0.07 catalyst using the dilute feed

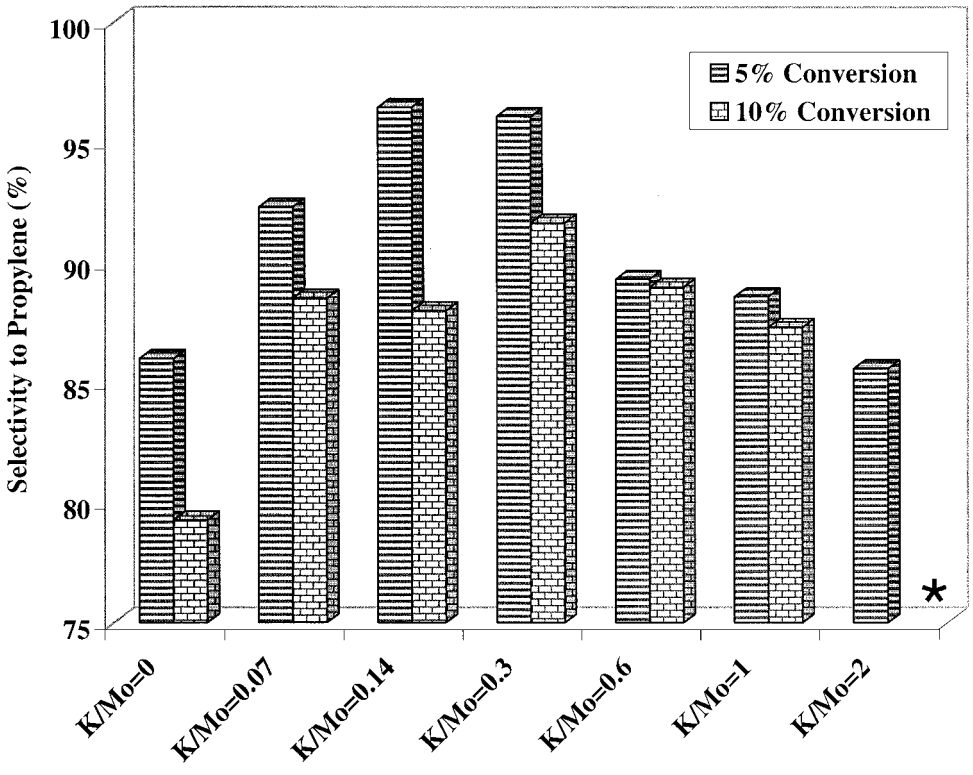

FIG. 6. Selectivity to propylene for 10% (K/Mo)/Si : Ti 1 : 1 catalysts at equal propane conversion (~5% and ~10%); 450°C; $\%N_2/C_3/O_2$, 61%/26%/13%; 25 cm^3/min. *, did not reach 10%.

concentration. Experiments were performed at 550°C and the residence time was varied from 0.6 to 10 s. The yield of propylene increased with increasing residence time, reaching a yield of ~30% at a residence time of ~5 s, where it leveled off and remained essentially unchanged with further increases in the residence time. Figure 8b shows the effect of residence time on the yield of other reaction products. While the yields of CO_2, C_2H_4, C_2H_6, and CH_4 all increase

TABLE 4

Selectivity Comparison for 10% (K/Mo)/Si : Ti 1 : 1 Catalysts with Different K/Mo Ratios at Equal Propane Conversion

	Selectivity (%)					
~5% Propane conversion	C_3H_6	CO_2	CO	C_2H_4	CH_4	C_2H_6
10% (Mo)/Si : Ti 1 : 1	86.0	5.6	8.4	0.1	0.0	0.0
10% (K/Mo = 0.07)/Si : Ti 1 : 1	92.3	5.5	2.2	0.1	0.0	0.0
10% (K/Mo = 0.14)/Si : Ti 1 : 1	96.5	3.2	0.3	0.1	0.0	0.0
10% (K/Mo = 0.3)/Si : Ti 1 : 1	96.1	3.2	0.5	0.1	0.1	0.0
10% (K/Mo = 0.6)/Si : Ti 1 : 1	89.3	10.2	0.0	0.5	0.0	0.0
10% (K/Mo = 1)/Si : Ti 1 : 1	88.5	10.6	0.0	0.4	0.1	0.4
10% (K/Mo = 2)/Si : Ti 1 : 1	85.6	10.0	0.0	2.5	2.0	0.0
	Selectivity (%)					
~10% Propane conversion	C_3H_6	CO_2	CO	C_2H_4	CH_4	C_2H_6
10% (Mo)/Si : Ti 1 : 1	79.3	7.0	13.6	0.1	0.0	0.0
10% (K/Mo = 0.07)/Si : Ti 1 : 1	88.5	5.0	6.4	0.1	0.0	0.0
10% (K/Mo = 0.14)/Si : Ti 1 : 1	88.0	7.5	4.3	0.1	0.1	0.0
10% (K/Mo = 0.3)/Si : Ti 1 : 1	91.7	4.9	3.3	0.1	0.0	0.0
10% (K/Mo = 0.6)/Si : Ti 1 : 1	89.0	7.4	0.0	2.4	1.3	0.0
10% (K/Mo = 1)/Si : Ti 1 : 1	87.3	6.8	0.0	3.3	2.6	0.0
10% (K/Mo = 2)/Si : Ti 1 : 1	Did not reach 10%					

Conditions: 450°C; $\%N_2/C_3/O_2$, 61/26/13; 25 cm^3/min.

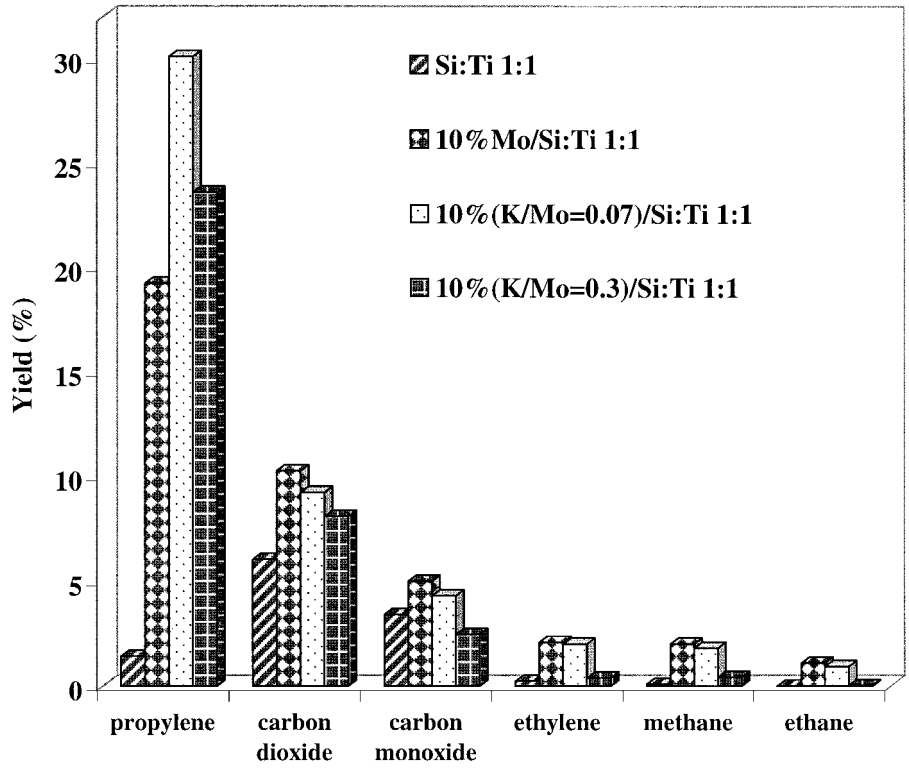

FIG. 7. Comparison between bare support and 10% Mo/Si : Ti 1 : 1 catalysts with K/Mo ratios of 0, 0.07, and 0.03 at dilute feed concentration; constant residence time (5 s); 550°C; %$N_2/C_3/O_2$, 92.5%/5%/2.5%.

with increasing residence time, the yield of CO does not show a clear trend.

A set of prehydrolyzed catalysts with a constant K/Mo ratio of 2 were compared to the "stoichiometrically" hydrolyzed catalyst with regard to their ODH behavior. Selectivities obtained at an equal conversion of ~3% and a temperature of 500°C are presented in Table 5. When the silica precursor is prehydrolyzed keeping the other synthesis parameters the same, we observe an appreciable increase in propylene selectivity compared to those of the catalysts prepared without any prehydrolysis step. However, changing the preparation parameters, such acidity or the speed of addition of the aqueous solutions for the prehydrolyzed catalyst, does not appear to have much effect on propylene selectivity. Another point worth noting about these comparisons is the fact that catalysts prepared without pH control (with or without prehydrolysis) show the lowest CO_2 and ethylene selectivities.

TABLE 5

Effect of Hydrolysis Conditions for 10% (K/Mo = 2)/Si : Ti 1 : 1 Catalysts

	Selectivity (%)					
	C_3H_6	CO_2	CO	C_2H_4	CH_4	C_2H_6
Hydrolyzed	83.2	15.5	0.0	1.1	0.1	0.0
Prehydrolyzed	90.0	8.6	0.0	1.4	0.0	0.0
Prehydrolyzed fast addition	73.5	24.2	0.0	2.2	0.0	0.0
Prehydrolyzed acidic (pH 3)	66.9	28.2	0.0	4.9	0.0	0.0
Prehydrolyzed basic (pH 11)	77.3	13.3	7.1	2.0	0.3	0.0

Conditions: ~3% propane conversion; 500°C; %$N_2/C_3/O_2$, 92.5/5/2.5; 25 cm^3/min.

To investigate the effect of the support composition, catalysts with different Si : Ti ratios were compared using 10% Mo loading and a K/Mo ratio of 2. The comparison was based on equal mass of Mo metal in the reactor. The temperature for these reactions was 550°C. The yields of different reaction products obtained are presented in Fig. 9. There was no C_2H_6 observed in these runs. The highest propylene yield was obtained over the catalysts that had a Si : Ti ratio of 1 : 1. This catalyst showed no CO or CH_4 formation and very little CO_2 and C_2H_4 formation. The Si-rich catalysts also appear to give relatively high yields for propylene, but these are accompanied by high yields for CO, CO_2, C_2H_4, and CH_4.

Homogeneous volume minimization downstream from reactor or free-radical quenching is necessary in propane ODH reaction to isolate catalytic activity from gas-phase activity. Radicals, once formed on the surface of the catalyst, can desorb during reaction and contribute to gas-phase pyrolysis downstream from the catalyst bed. This "surface-assisted or surface-initiated gas-phase reaction" that can occur in ODH of propane has been studied by Burch and Crabb (30) and modeled by Nguyen and Kung (31). To examine the contribution of homogeneous

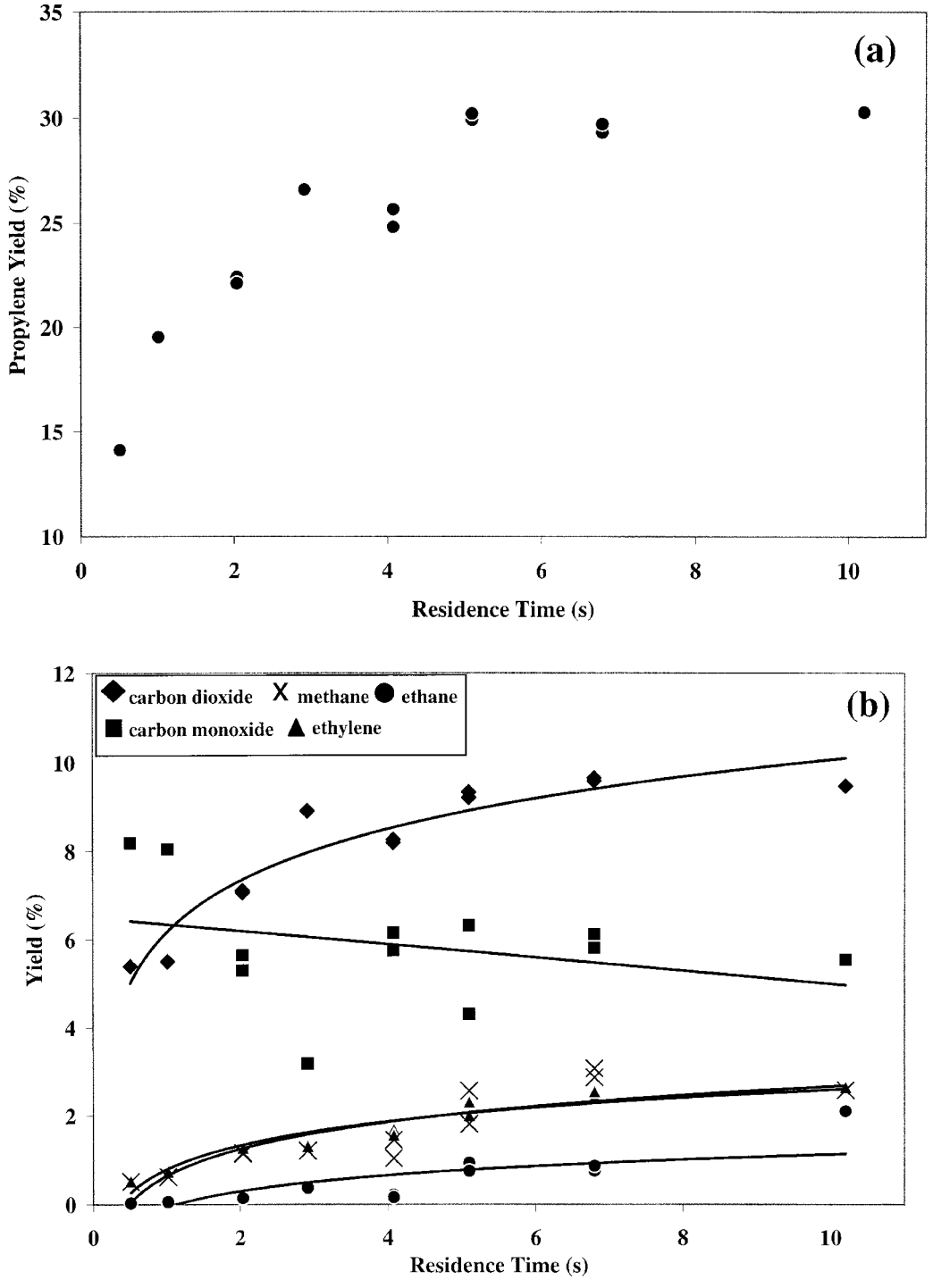

FIG. 8. Effect of feed residence time on (a) propylene yield and (b) product distribution over 10% (K/Mo = 0.07)/Si : Ti 1 : 1; constant Mo loading (0.1 g); 550°C; $\%N_2/C_3/O_2$, 92.5%/5%/2.5%.

reaction, experiments were performed with and without dead-volume packing downstream from the reactor. Our results showed this effect to be important even at 400°C. Experiments performed using the K/Mo = 0.07 catalyst and a feed stream ($\%N_2/C_3/O_2$, 92.5%/5%/2.5%) of 25 cm^3/min flow rate showed that the propane conversion increased from 13 to 16% when packing downstream from the catalyst bed was removed. In all our runs, a great deal of attention

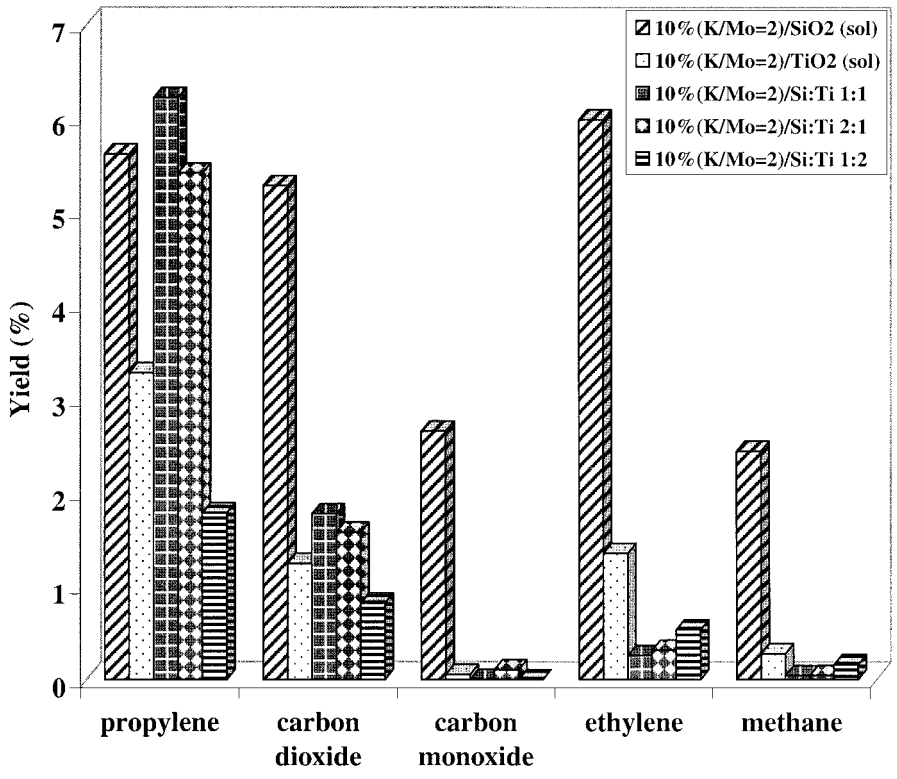

FIG. 9. Effect of support Si : Ti molar ratio of 10% (K/Mo = 2) loaded catalysts on yield; constant Mo loading (0.1 g); 550°C; $\%N_2/C_3/O_2$, 92.5%/5%/2.5%; 25 cm^3/min.

was paid to minimizing the gas-phase reaction contribution. The measures we took include raising the catalyst bed, using a quartz wool packing to minimize the homogeneous volume downstream from the reactor and providing rapid quenching in the post-catalyst bed region. Care was also taken to eliminate "hot spots" or temperature effects by using very small catalyst particles, small catalyst bed volumes, and large percentages of the inert gas (N_2) compared to propane and oxygen concentrations. While the contribution from non-oxidative dehydrogenation needs to be taken into consideration, the very low yields we saw for methane, and the balances for carbon, hydrogen, and oxygen, which were ~100% for the reactions, lead us to conclude that this contribution is negligible. The findings of Burch and Crabb (30), which showed that the nonoxidative dehydrogenation became appreciable only at temperatures close to 700°C, also support this assumption. Although care was taken to isolate the catalytic activity for the oxidative reaction, contributions from gas-phase reactions cannot be completely ruled out.

3.3. NH_3 Adsorption

The IR spectra of ammonia species formed on 10% Mo/Si : Ti 1 : 1 catalysts with different K/Mo ratios are shown in Fig. 10. The bands listed in Table 6 characterize the spectra. Bands commonly used to characterize Lewis and Brønsted acidity are those located at ~1607 (Lewis) and ~1448 cm^{-1} (Brønsted). In Table 6, an attempt to quantify the Lewis and Brønsted characteristics of the catalysts is

TABLE 6

NH_3 IR Adsorption Bands

Band (cm^{-1})	Acidity	Assignment
1074–1082	H-Bonded NH_3	NH_2 Rocking
1220–1248	Lewis	N–N Streching
1450–1434	Brønsted	NH_2 Wagging
1604–1607	Lewis	NH_2 Scissoring
1670–1680	Brønsted	NH_2 Scissoring

	Baseline-corrected peak areas			
K/Mo Ratio	Lewis, ~1607 cm^{-1}	Brønsted, ~1448 cm^{-1}	Area B/area L	%Lewis[a]
Si : Ti 1 : 1	6.4	26.1	4.1	20
0	6.8	42.4	6.3	14
0.07	1.3	32.7	25.0	4
0.3	5.1	34.0	6.6	13
0.6	1.1	9.4	8.8	10
2	5.7	15.3	2.7	27

[a] Calculated with peak areas.

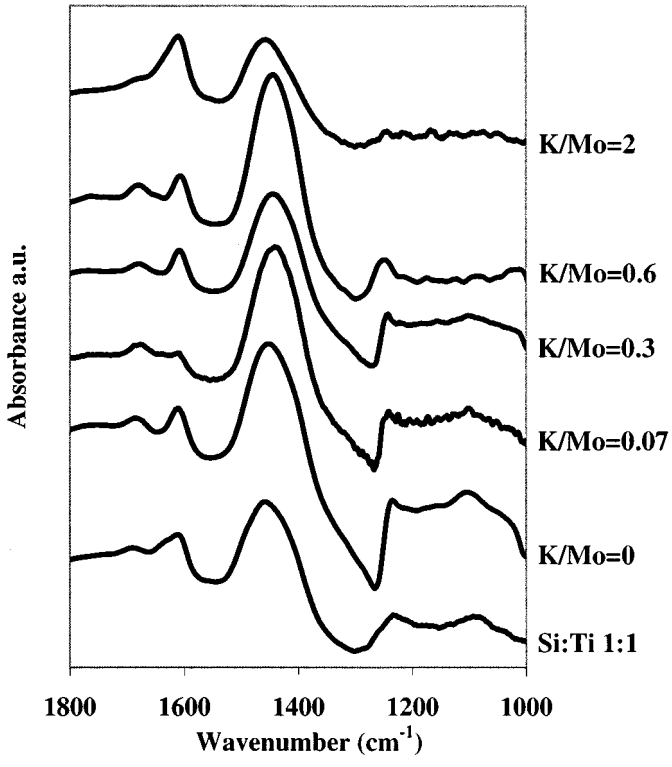

FIG. 10. Adsorbed NH_3 IR bands over 10% Mo/Si : Ti 1 : 1 catalysts with different K/Mo ratios and bare support.

made using these peak areas and intensities. Compared to the Si : Ti support, the K/Mo = 0 catalyst has considerably more Brønsted acid character and similar Lewis acid character. With the addition of potassium to the catalyst, the Lewis acid character decreases to a minimum at K/Mo = 0.07 and sharply increases at K/Mo = 2.

3.4. TPR

Temperature-programmed reduction experiments were performed on catalysts with different K/Mo ratios. The results are compared to those of bulk MoO_3 and K_2MoO_4 samples prepared from the same precursors as the synthesized catalysts. The results are plotted in Fig. 11. The profiles for supported K/Mo catalysts are similar, consisting of one major temperature maximum in the 400–500°C range. As the K/Mo ratio increases, the maxima begin to shift to higher temperatures and the peaks show considerable broadening. At K/Mo ratios of 0.6 and higher, we begin to see peaks becoming very noticeably asymmetrical, possibly representing two different reduction sites. When these profiles are compared to that of bulk K_2MoO_4, we see that the temperature for this secondary feature, which appears as a large shoulder, coincides with the major reduction peak observed over the bulk K_2MoO_4. Table 7 summarizes the

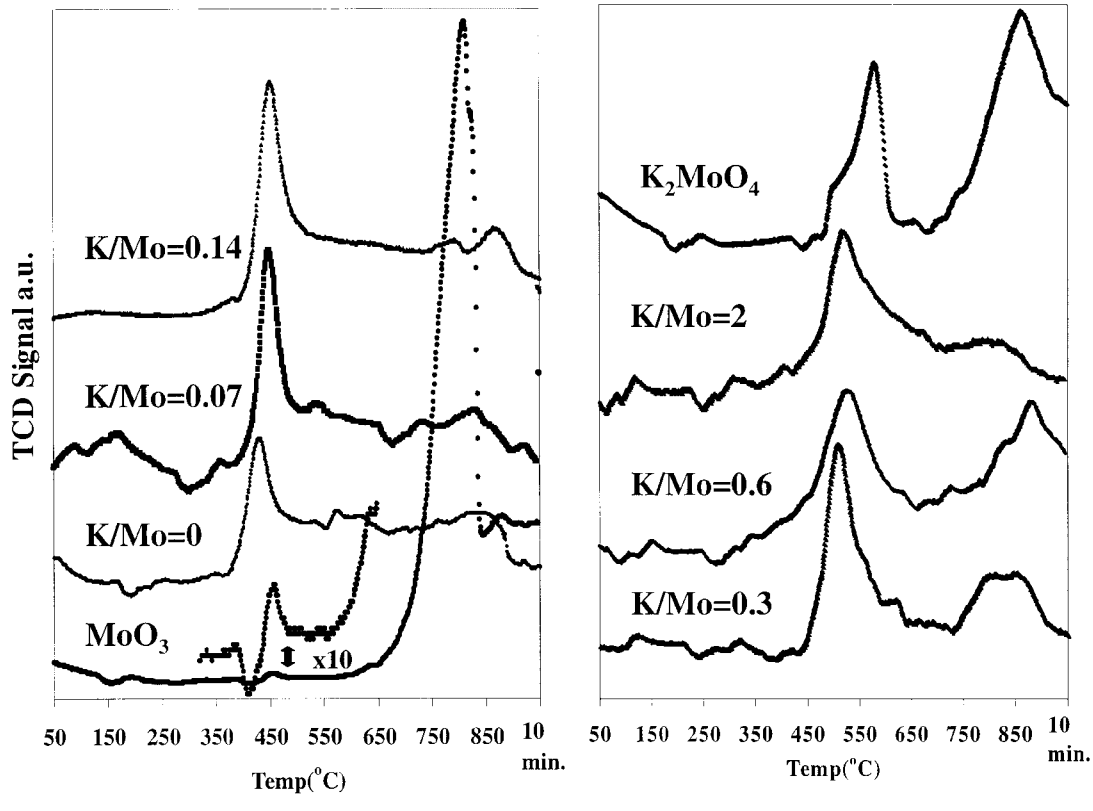

FIG. 11. Temperature-programmed reduction profiles for 10% Mo/Si : Ti 1 : 1 catalysts with different K/Mo ratios; 10% H_2/N_2.

TABLE 7

Temperature-Programmed Reduction of 10% (K/Mo)/Si : Ti 1 : 1 Catalysts with Different K/Mo Ratios

Catalyst	1st peak maxima (°C)[a]	FWHM (°C)
MoO_3	459	34
K/Mo = 0	436	58
K/Mo = 0.07	450	46
K/Mo = 0.14	456	53
K/Mo = 0.3	512, 560sh	75
K/Mo = 0.6	531, 566sh	104
K/Mo = 2	520, 570sh	118
K_2MoO_4	581	54

[a] sh = shoulder.

temperature maxima and the FWHM (full width at half-maximum) of these major reduction peaks.

3.5. Propane TPD

Analysis of the desorbed species after propane adsorption showed propane, propylene, water, CO_2, CO, O_2, and trace amounts of methane, ethane, and acrolein desorbing from the surface. Propylene desorption profiles for the Si : Ti 1 : 1 support, 10% Mo/Si : Ti 1 : 1, and potassium-containing catalysts of K/Mo = 0.07 and 0.3 are plotted in Fig. 12. Focusing on the "molybdenum only" catalyst, there is one desorption feature with peak maximum temperature around 200°C. An important aspect of these profiles is that the first desorption feature shifts to lower temperatures with increasing potassium loading. The water desorption profiles follow the propylene desorption closely, indicating that propylene formation takes place oxidatively, using the lattice oxygen. The shift of the propylene desorption peaks to lower temperatures also points to an ease of desorption from the surface for the potassium-containing catalysts. With the addition of potassium, two additional sites for propylene desorption are formed on the K/Mo = 0.3 catalyst at higher temperatures (~260 and ~300°C). The desorption profiles for carbon monoxide for the same catalysts are plotted in Fig. 13. Although ethylene has the same molecular weight as carbon monoxide, by following fragments created by both, we determined that the first desorption peaks (<200°C) are associated with ethylene desorption and the remainder of the profile belongs to carbon monoxide alone. There are three significant desorption features present on the "molybdenum only" catalyst at 360, 465, and 650°C. With the addition of potassium, these desorption features appear to be suppressed and less pronounced in a broad profile.

3.6. In Situ DRIFT Spectra

To ascertain the differences in reaction intermediates present on the catalyst during reaction conditions, IR spectra of adsorbed species were obtained at 450°C surface

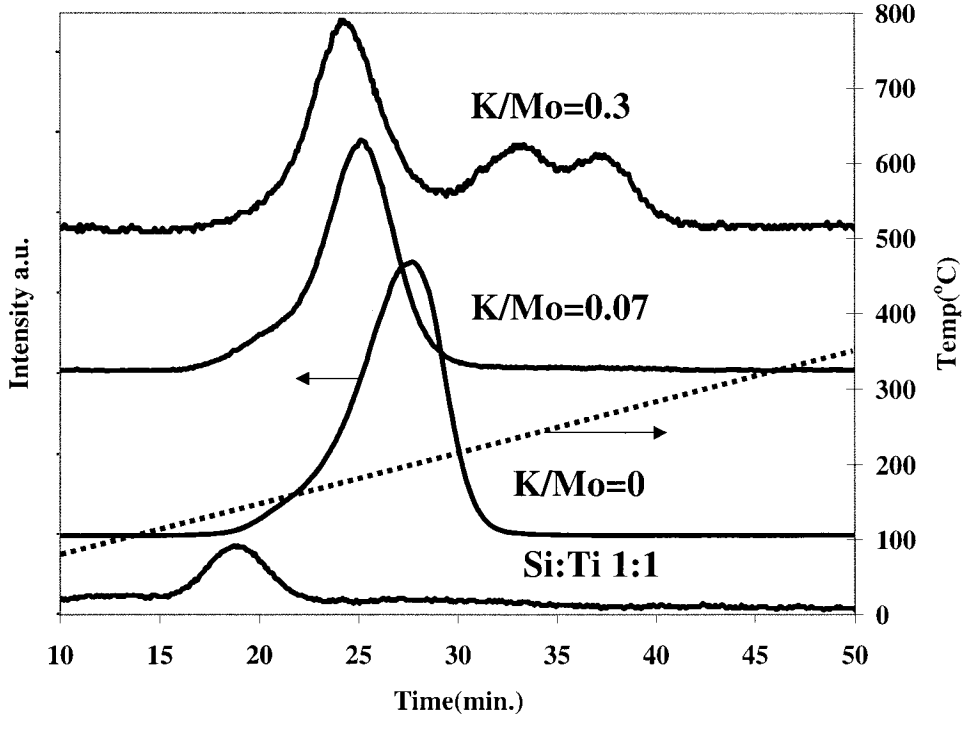

FIG. 12. Propane temperature-programmed desorption: propylene desorption profiles over bare support and 10% Mo/Si : Ti 1 : 1 catalysts with K/Mo ratios of 0, 0.07, and 0.03.

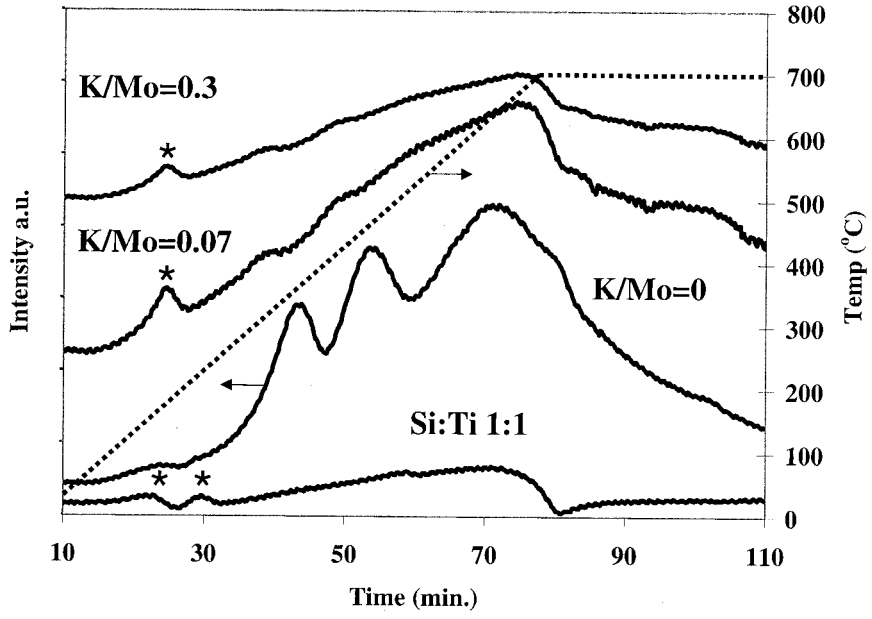

FIG. 13. Propane temperature-programmed desorption: carbon monoxide desorption profiles over bare support and 10% Mo/Si : Ti 1 : 1 catalysts with K/Mo ratios of 0, 0.07, and 0.03 (∗, ethylene desorption).

temperature. After gas-phase spectra subtraction, the results are plotted in Fig. 14a for the range 1800–1300 cm^{-1}. Similar bands are observed on the K/Mo catalysts studied. The band observed around 1689 cm^{-1} is associated with adsorbed acetone. Bands located around 1540, 1503, 1430, 1360, and 1328–1336 cm^{-1} are associated with acetate, formate, π-allyl, and acrolein type species (32–40). Olefinic CH_x stretches are located at 1458 and 1390 cm^{-1}. Two interesting features to note in Fig. 15a are that the highest yield ODH catalyst of this study, K/Mo = 0.07, shows the most intense olefinic CH_x stretching bands. Furthermore, one of the most selective ODH catalysts, K/Mo = 0.3, shows a lack of intensity from the acetate and formate species present on the other catalysts. This agrees well with the reaction

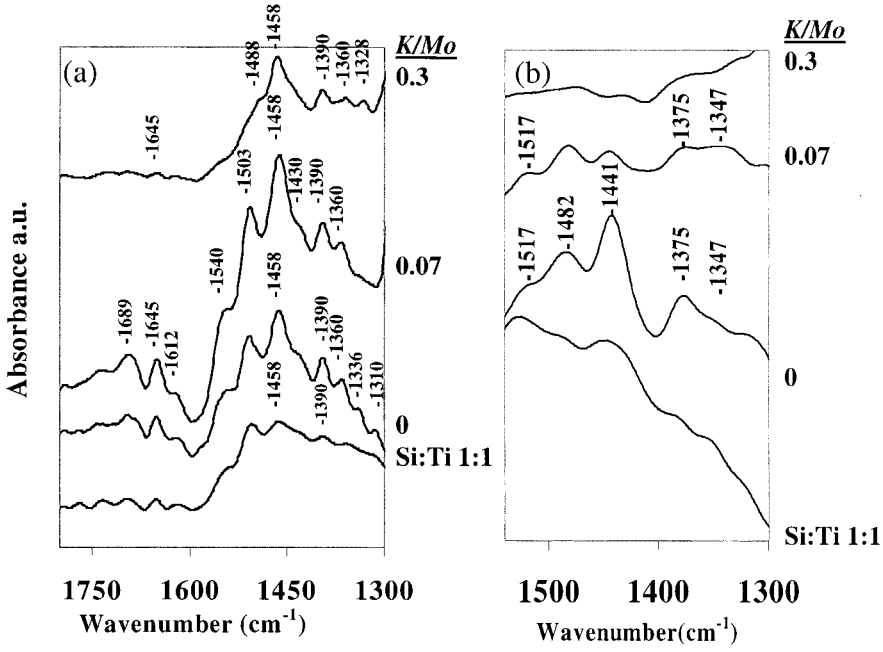

FIG. 14. (a) *In situ* DRIFT spectra of over bare support and 10% Mo/Si : Ti 1 : 1 catalysts with K/Mo ratios of 0, 0.07, and 0.03; 450°C surface temperature; $\%N_2/C_3/O_2$, 61%/26%/13%. (b) DRIFT spectra after quenching under N_2.

results as these intermediates may lead to the formation of CO_x products. In Fig. 14b, the IR spectra are shown after the reaction has been quenched to room temperature under nitrogen. It is apparent that olefinic species are still present on the "molybdenum only" catalyst, indicated by the bands at 1441 and 1375 cm^{-1}, which have shifted to lower wavenumbers with the decrease in temperature of the sample surface. Over the potassium-containing catalysts, on the other hand, these bands have essentially disappeared. Again, this suggests a weaker adsorption of propylene on the surface, leading to easier desorption.

4. DISCUSSION

In this study, we have examined the ODH of propane over K/Mo catalysts supported on Si : Ti mixed oxides prepared by a "one-pot" sol–gel/coprecipitation technique. The catalysts prepared had well-dispersed Mo species on the surface existing either in an octahedral molybdenum oxide matrix or in a tetrahedral K–molybdate matrix. As the K/Mo ratio was increased, the latter species increased at the expense of the former, leading to a complete incorporation of the Mo species in the molybdate matrix when the K/Mo ratio reached 2. This catalyst behaved quite differently than the catalysts with lower K/Mo ratios, partly due to the lack of synergy that existed between the two phases on the surface. Propane ODH reaction experiments were performed with two different feed conditions. When the more dilute feed mixtures (5% propane) were used, high propylene yields (up to 30%) were obtained over catalysts with K/Mo ratios less than 0.6. The reaction studies over the same catalysts with higher propane concentrations (26%) did not lead to as high yields, but had the advantage of giving higher concentrations of propylene in the product stream.

Catalyst comparisons done using equal surface area experiments or equal conversion experiments showed a maximum in propylene yield with increasing K/Mo ratios. The performance of 10% (K/Mo)/Si : Ti 1 : 1 catalysts in ODH exhibited the alkali doping effect reported for several types of catalysts, that is, an initial increase in selectivity or activity and a sharper decrease as larger quantities of alkali are added. Jiang *et al.* have seen the same K–Mo interaction on a γ-Al_2O_3-supported catalyst for alcohol synthesis from syngas (41). They found a parallel between the activity for alcohol formation and the formation of K–Mo species (K-containing $Mo_7O_{24}^{6-}$ units). This effect was maximized at a K/Mo ratio of 0.8. They have also shown, from TPR and Raman results, that several types of Mo(VI) oxidic species are present on their K/Mo catalyst (K/Mo = 0.35). With the interaction of Mo(VI) with K, supported Mo species can lose coordinated oxygen during calcination and be converted to Mo(V). This effect can also take place on a TiO_2 support (42). This theory is consistent with Mo(V) being most active for molybdate catalysts in ODH reactions frequently cited in the literature. Furthermore, Erdohelyi *et al.* have also seen the presence of Mo(V) on K-promoted Mo/SiO_2 catalysts for the partial oxidation of ethane (43). Kantschewa *et al.* (44) have shown a strong interaction between K and Mo where the reducibility of a $NiMo/\gamma$-Al_2O_3 catalyst was suppressed with the addition of K. Our TPR results, which show a shift of the reduction maxima to higher temperatures with the addition of potassium, are consistent with these findings in the literature, which point to a strong relationship between the reduction behavior of the catalyst and the extent of alkali doping. It is conceivable that potassium is suppressing the reducibility of the molybdenum species at low K/Mo ratios and stabilizing the Mo(V) oxidation state.

In addition to affecting the reducibility of molybdenum species, it is possible that the presence of alkali dopants also influences the acidity of the catalysts. Abello *et al.* have reported an acidity–adsorption strength relation on their K/Mo catalyst in the ODH reaction (10). In our ammonia adsorption experiments, it should be noted that the catalyst that gives the highest propylene yield (K/Mo = 0.07) exhibits the lowest Lewis acidity as determined by IR bands of coordinated NH_3 species. The Brønsted centers, on the other hand, are quantified by the IR bands associated with ammonium ions (NH_4^+), which form on M–OH sites, where *M* is a metal center. It is interesting that the catalyst which gives the highest propylene yield has also the highest Brønsted-to-Lewis ratio. Another interesting point about these results is that this ratio is higher on the bare support than it is over the high K content catalysts (K/Mo > 1). If the Brønsted centers can activate the alkane and if the Lewis sites provide strong adsorption sites for the olefin, then this result could help to explain why the bare Si : Ti support gave a higher propylene yield than catalysts with high K/Mo ratios in higher propane concentration experiments. The fact that this ratio is lower over the support than it is over the Mo-only catalyst is consistent with this argument, since the propylene yield is lower over the former than it is over the latter.

Pantazidis *et al.* have noted that a good balance between acidity and reducibility is needed over VMgO catalysts in the ODH of propane (45). O'Young has studied the reducibility of Mo/γ-Al_2O_3 catalysts with the addition of potassium and cesium (46) and has shown two levels of alkali/Mo interaction. One appears at alkali/Mo < 1, where the reducibility of Mo is only slightly affected. The other interaction type occurs at alkali/Mo > 1, where the reducibility of the catalyst is significantly suppressed. This could offer an explanation for the very low activity observed over the catalysts with K/Mo ratios greater than 1, especially for the K/Mo = 2 catalyst. When explaining the very low activity observed over the K/Mo = 2 catalyst, one needs to consider the fact that all of the Mo over this catalyst exists in a K_2MoO_4 matrix, and, as seen in the XPS data, there are

no surface-coordinated Mo oxide species. This catalyst is likely to behave quite differently than a catalyst with both molybdenum oxide and molybdate species present on its surface.

There is also evidence in the literature pointing to electronic properties of molybdenum being sufficiently altered by the presence of K to affect its adsorption behavior. In this study, *in situ* IR spectra results of K/Mo catalysts (Figs. 14a and 14b) together with propane TPD (Fig. 12) indicate that the addition of potassium is affecting how strongly propylene is held on the surface of the catalyst. Both sets of experiments show propylene desorbing from the K-containing catalyst surfaces much more easily compared to the potassium-free catalysts. Especially worth noting is the fact that, during reaction, the K-containing catalysts exhibit the highest intensity for olefinic species in the DRIFTS spectra but, once quenched and flushed, lose these species completely. On the other hand, the potassium-free catalysts show that these species continue to exist on the surface, even after quenching and flushing. Another interesting observation from our studies is related to the oxidation behavior of the catalysts. *In situ* IR spectra show a much weaker intensity for the oxygen-containing intermediates over the K-containing catalysts than Mo-only catalyst. This is in good agreement with the reaction data, which show a product distribution favoring ODH products more than complete oxidation products over the potassium-doped catalysts. Propane TPD experiments also show that the lattice oxygen availability for carbon monoxide formation is suppressed with the addition of potassium to the catalyst (Fig. 13).

The catalyst characterization studies indicate that there are additional factors that control catalytic behavior besides the alkali dopants present. In particular, the sol–gel parameters are seen to affect the structural characteristics of the catalysts. The K/Mo = 2 catalysts prepared by prehydrolysis of the silica precursor offer a higher selectivity at equal conversion levels (Table 5), possibly due to the increased Si–Ti connectivity achieved in this procedure compared to the preparation method which uses simultaneous hydrolysis of the two precursor. In our preparation experiments, some differences observed in catalyst structure when K/Mo ratio is varied may actually be the result of pH variation caused by the amount of alkali added to the sol–gel medium. Our XPS data, laser Raman spectra, and X-ray diffraction patterns indicate that as more potassium is added to the catalysts, titania species turn from small domains with a high Si–Ti connectivity to segregated anatase-like structures. This structural difference, which may be due to the higher pH of the synthesis medium with increasing potassium doping, may change the catalyst performance by affecting the anatase-to-rutile phase transition and by influencing the oxygen mobility of the support. Another property which is strongly affected by the hydrolysis parameters is the surface area. The pH of the medium has two opposing effects on the surface area. On one hand, the acidic preparation can increase the surface area of the catalyst by making thinner gels, smaller particles, and increasing the hydrolysis rates. On the other hand, the basic conditions during preparation can also increase surface area by forming a more porous structure by increasing condensation rates (24). This may partly explain the decrease followed by an increase that we observed in the surface area with increasing K/Mo ratio. The pH of the preparation medium not only affects the support structure, but it also has a strong effect on the type of molybdena species that are formed on the surface. This is due to the strong effect of the pH on the state of agglomeration of molybdenum species in aqueous media (47). In the acidic solutions, polymerization of molybdenum species takes place, forming $Mo_7O_{24}^{6-}$ type species. In alkaline solutions, however, the tetrahedral MoO_4^{2-} species predominate. During precipitation, these species are more likely to be incorporated into the K_2MoO_4 matrix, while the polymerized species mostly form surface-coordinated Mo oxide species. The Raman spectroscopy results that showed potassium molybdate species present on catalysts K/Mo = 0.6 and 1.0 is consistent with this argument. The presence of K_2MoO_4 as a three-dimensional phase on the surface can also help to explain the lower surface area of these catalysts.

When we discuss a balance in reducibility and acidic/basic characteristics of catalysts in the ODH of propane, it is necessary to think in terms of the relative rates of the kinetic steps occurring on oxide catalysts. As discussed by Kung in a review article (2), one needs to consider the two reactions, namely propane → propylene and propylene → CO_x. It was shown that, perhaps on all catalysts, the rate for the second reaction could be 5 to 10 times higher than that of the first reaction. Recently, work by Khodakov *et al.* has begun to answer these fundamental questions by measuring the relative rates of propylene and CO_x formation by residence time and isotopic tracer experiments (49). Furthermore, they have commented on the likelihood of similar active sites being responsible for both reactions. In these terms, it seems that the promotion effect of potassium combined with the unique state of the titania in the Si : Ti mixed oxide support needs to be considered in explaining the higher yields obtained over these catalysts. When the selectivity is considered in terms of these two competing reactions, it becomes clearer that both the reducibility and oxygen mobility characteristics of the catalyst, and its acidity, need to be simultaneously taken into account. While the surface oxygen species affect the rates of both reactions, it is conceivable that a catalyst with a strong Lewis character will have a higher affinity for the electron-rich double bond of propylene, leading to its further oxidation before it desorbs from the surface.

ACKNOWLEDGMENTS

Financial support provided by the National Science Foundation (Grant CTS-9412544) is gratefully acknowledged. The authors also thank Dr. Gurkan Karakas for his technical assistance at the early stages of the project.

REFERENCES

1. Peaff, G., *Chem. Eng. News* **Jan 16**, 16 (1995).
2. Kung, H. H., *Adv. Catal.* **40**, 1 (1994)
3. Cavani, F., and Trifiro, F., *Catal. Today* **24**, 307 (1995).
4. Stern, D. L., and Grasselli, R., *J. Catal.* **167**, 550 (1997).
5. Meunier, F. C., Yasmeen, A., and Ross, J. R. H., *Catal. Today* **37**, 33 (1997).
6. Driscoll, S. A., Gardner, D. K., and Ozkan, U. S., *J. Catal.* **147**, 379 (1994).
7. Erdohelyi, A., Mate, F., and Solymosi, F., *J. Catal.* **135**, 563 (1992).
8. Akimoto, M., and Echigoya, E., *J. Catal.* **35**, 278 (1974).
9. Mross, W. D., *Catal. Rev.-Sci. Eng.* **25**(4), 591 (1983).
10. Abello, M. C., Gomez, M. F., and Cadus, L. E., *Catal. Lett.* **53**, 53 (1998).
11. Notari, B., *Adv. Catal.* **41**, 253 (1996).
12. Stakheev, A. Y., Shipiro, E. S., and Apijok, J., *J. Phys. Chem.* **97**, 5668 (1993).
13. Lassaletta, G., Fernandez, A., Espinos, J. P., and Gonzalez-Elipe, A. R., *J. Phys. Chem.* **99**, 1484 (1995).
14. Walters, J. K., Rigden, J. S., Dirken, P. J., Smith, M. E., Howells, W. S., and Newport, R. J., *Chem. Phys. Lett.* **264**, 539 (1997).
15. Kumar, S. R., Suresh, C., Vasudevan, A. K., Suja, N. R., Mukundan, P., and Warrier, K. G. K., *Mater. Lett.* **38**, 161 (1999).
16. Klein, S., Thorimbert, S., and Maier, W. F., *J. Catal.* **163**, 476 (1996).
17. Liu, Z., Tabora, J., and Davis, R. J., *J. Catal.* **149**, 117 (1994).
18. Baiker, A., Dollenmeier, P., and Glinski, M., *Appl. Catal. A* **35**, 365 (1987).
19. Vogt, E. T. C., Boot, A., van Dillen, A. J., Guess, J. W., Janssen, F. J. J. G., and van den Kerkhof, F. M. G., *J. Catal.* **114**, 313 (1988).
20. Udomsak, S., and Anthony, R. G., *Ind. Eng. Chem. Res.* **35**, 47 (1996).
21. Rieck, J. S., and Bell, A. T., *J. Catal.* **99**, 262 (1986).
22. Feng, Z., Liu, L., and Anthony, R. G., *J. Catal.* **136**, 423 (1993).
23. Ozkan, U. S., Cai, Y., Kumthekar, M. W., and Zhang, L., *J. Catal.* **142**, 182 (1993).
24. Brinker, C. J., and Scherer, D. W., "Sol-Gel Science." Academic Press, New York, 1990.
25. Izutsu, H., Nair, P. K., Maeda, K., Kiyozumi, Y., and Mizukami, F., *Mater. Res. Bull.* **32**, 1303 (1997).
26. Wachs, I. E., *Catal. Today* **27**, 437 (1996).
27. Erdohelyi, A., Fodor, K., and Solymosi, F., *J. Catal.* **166**, 244 (1997).
28. Stakheev, A. Y., Shpiro, E. S., and Apijok, J., *J. Phys. Chem.* **97**, 5668 (1993).
29. Parmaliana, A., Sokolovski, V., Miceli, D., and Giordano, N., *Appl. Catal. A* **135**, L1 (1996).
30. Burch, R., and Crabb, E. M., *Appl. Catal. A* **100**, 111 (1993).
31. Nguyen, K. T., and Kung, H. H., *J. Catal.* **122**, 415 (1990).
32. Matyshak, V. A., and Krylov, O. V., *Catal. Today* **25**, 1 (1995).
33. Busca, G., Finocchio, E., Lorenzelli, V., Ramis, G., and Baldi, M., *Catal. Today* **49**, 453 (1999).
34. Baldi, M., Milella, F., Ramis, G., Escribano, V. S., and Busca, G., *Appl. Catal. A* **166**, 75 (1998).
35. Dandekar, A., and Vannice, M. A., *J. Catal.* **183**, 344 (1999).
36. Centi, G., and Perathoner, S., *Appl. Catal. A* **124**, 317 (1995).
37. Poignant, F., Saussey, J., Lavalley, J.-C., and Mabilon, G., *Catal. Today* **29**, 93 (1996).
38. Bamwenda, G., Ogata, A., Obuchi, A., Takahashi, H., and Mizuno, K., *React. Kinet. Catal. Lett.* **56**, 311 (1995).
39. Guglielminotti, E., and Boccuzzi, F., *J. Mol. Catal. A* **104**, 273 (1996).
40. Martin, C., Martin, I., and Rives, V., *J. Chem. Soc., Faraday Trans.* **89**, 4131 (1993).
41. Jiang, M., Bian, G. H., and Fu, Y. L., *J. Catal.* **147**, 144 (1994).
42. Caceres, C. V., Fierro, L. G., Lazaro, J., Agudo, A. L., and Soria, J., *J. Catal.* **122**, 113 (1990).
43. Erdohelyi, A., Mate, F., and Solymosi, F., *Catal. Lett.* **8**, 229 (1991).
44. Kantschewa, M., Delannay, F., Jeziorowski, H., Delgado, E., Eder, S., Ertl, G., and Knozinger, H., *J. Catal.* **87**, 482 (1984).
45. Pantazidis, A., Auroux, A., Herrmann, J.-M., and Mirodatos, C., *Catal. Today* **32**, 81 (1996).
46. O'Young, C. L., *J. Phys. Chem.* **93**, 2016 (1989).
47. Ozkan, U., and Schrader, G. L., *J. Catal.* **95**, 120 (1985).
48. Lassaletta, G., Fernandez, A., Espinos, J. P., and Gonzalez-Elipe, A. R., *J. Phys. Chem.* **99**, 1484 (1995).
49. Khodakov, A., Olthof, B., Bell, A. T., and Iglesia, E., *J. Catal.* **181**, 205 (1999).